Optical spectroscopy on implanted and annealed silicon wafers: Plasma resonance wavelength

Constantinos Christofides
Department of Natural Sciences, Faculty of Pure and Applied Sciences, University of Cyprus, P. O. Box 537, Nicosia, Cyprus

Andreas Othonos
Ontario Laser and Lightwave Research Center, University of Toronto, Toronto, Ontario M5S 1A7, Canada

Michel Bisson
MITEL, Semiconductor Division, 18 Boulevard de l'Aeroport, Bromont, Québec JOE ILO, Canada

Joumana Boussey-Said
Laboratoire de Physique des Composants à Semiconducteur, URA CNRS 840, 23 Rue des Martyrs, B. P. 257, 38031 Grenoble Cedex 1, France

(Received 25 August 1993; accepted for publication 19 November 1993)

A study of the effects of annealing temperature on phosphorus-implanted silicon films is carried out. Fourier transform infrared spectroscopy has been performed with two different instruments in the spectral ranges of 0.75–4 μm and 3–25 μm. In the first spectrum range special attention was given to the influence of implantation dose on reflectivity. The minimum reflectivity associated with plasma resonance has been fully employed for estimation of the electrical activation of implanted impurities. Other conclusions concerning the activation of free carriers (implanted impurities) with implantation dose and annealing temperature have been reached.

I. INTRODUCTION

During the last few decades various types of measurements have been used for the characterization of implanted wafers.[1] Generally, the aim of experimental characterization of such materials is to quantify four important effects of the ion implantation and annealing process: (a) the induced damage (short and long-range disorder); (b) spatial distribution profiles of the damage; (c) kinetics of annihilation mechanisms; and (d) electrical activation of the implanted impurities.

Fourier transform infrared (FTIR) spectroscopic measurements have the advantage of giving quantitative and qualitative information concerning the above four aspects in implanted (unannealed and annealed) semiconducting wafers. In addition, they represent a nondestructive and contactless technique. For this reason FTIR spectroscopy has been adopted by several groups around the world for the characterization of such materials.

During the mid 70's, Kachare *et al.* performed normal incidence reflection and transmission measurements of GaAs and GaP implanted wafers at high doses ($\Phi=1\times10^{17}$ cm^{-2}) and energies ($E=3$ MeV).[2,3] By using the same technique Wang *et al.*[4] studied the effect of annealing on the optical properties of implanted Ge. Infrared studies on heavily implanted phosphorus ($E=0.2$–2.7 MeV and $\Phi=10^{16}$–10^{17} P$^+$/cm^2) have also been performed in order to study the thickness as well as the refractive indices of such implanted layers.[5] Infrared spectroscopy on Be-implanted GaAs has also been performed.[6] Refractive index profiles and range distribution of silicon implanted with high energy nitrogen has been studied by Hubler *et al.*[7] It is also important to note that other researchers such as Fredrickson *et al.*,[8] Waddell *et al.*,[9] and Spitzer *et al.*[10] have used similar techniques for the characterization of implanted semiconducting wafers. Finally, one can cite the work of Tatarkiewicz whose excellent review paper in optical effects of high energy implantations in semiconductors, published in 1989, describes optical effects in high energy implanted semiconducting wafers.[11]

This work differs from previous investigations for four main reasons: (i) Unlike the majority of studies carried out until today, our spectroscopic measurements were performed on wafers implanted at the order of keV as opposed to MeV; (ii) the implanted samples were annealed systematically in a wide range of temperatures; (iii) special attention was given to the annealing kinetics of defects; (iv) a model presented by Schumann and Phillips[12] was used for the first time toward the characterization of implanted and high temperature annealed materials. This model was used to estimate the activation of implanted impurities versus annealing temperature, T_a.

Finally, details about the implanted samples are given in Sec. II, Sec. III summarizes the experimental results, while Sec. IV presents a useful theoretical background. The theoretical model is used in Sec. V to estimate the degree of activation of implanted impurities.

II. IMPLANTED SILICON SAMPLES

2-in.-diam silicon wafers lightly doped with boron (20–25 Ω cm) were implanted with phosphorus at various doses ($\Phi=1\times10^{13}$ to 1×10^{16} P$^+$/cm^2 and $E=150$ keV) through a thin oxide layer at room temperature. The implantation process was done by MITEL Semiconductor Division at Bromont, Québec, Canada in 1992. After implantation the wafers were cut with an automatic diamond

 0021-8979/94/75(7)/3377/8/$6.00

TABLE I. Junction's depths of samples implanted with 150 keV at various doses [$\Phi(P^+/cm^2)$], unannealed and annealed at various annealing temperatures [T_a(°C)]. The values of the first lines for each annealing temperature has been obtained from 1D-SUPREM III simulation (d_s) while second lines (in bold) were obtained from spreading resistance measurements (d_R). NA: nonannealed.

$\Phi(P^+/cm^2)$ T_a(°C)	1×10^{13}	1×10^{14}	5×10^{14}	1×10^{15}	5×10^{15}	1×10^{16}
NA	0.45	0.48	0.50	0.51	0.52	0.53
800	0.45	0.50	0.52	0.53	0.63	0.63
	0.48	**0.64**	**0.65**	**0.63**	**0.75**	**0.69**
850	0.46	0.49	0.53	0.52	0.75	0.80
	0.50	**0.65**	**0.65**	**0.67**	**0.80**	**0.80**
900	0.48	0.50	0.54	0.55	0.90	1.02
	0.60	**0.80**	**0.70**	**0.70**	**0.90**	**1.01**
950	0.53	0.57	0.60	0.60	0.97	1.45
	0.60	**0.85**	**0.80**	**0.75**	**1.10**	**1.50**
1000	0.63	0.72	0.75	0.78	0.97	1.90
	0.68	**0.90**	**0.90**	**0.80**	**1.30**	**1.50**
1100	1.32	1.55	1.70	1.74	2.03	2.40
	0.80	**1.15**	**1.51**	**1.52**	**1.81**	**2.60**

cutter along the crystallographic axes into several samples of dimensions 1 cm×1 cm. These samples were then thermally annealed isochronically at various temperatures: T_a (300, 350, 400, 500, 550, 600, 700, 800, 850, 900, 950, 1000, and 1100 °C) for 1 h in an inert nitrogen atmosphere. After annealing, the oxide overlayer was etched away and the samples were used for FTIR spectroscopic characterization.

III. EXPERIMENTAL RESULTS

A. FTIR measurement between 0.75 and 4.0 μm

In this section we present FTIR reflection and transmission spectra (R for reflection and T for transmission) for the implanted samples described in Table I. As it was expected, for very lightly implanted samples (1×10^{13} P^+/cm^2) the difference between the reflection spectra of low and high annealing temperatures is not significant.

Figures 1(a)–1(e) present several FTIR reflective spectra obtained at room temperature in the range of 0.75–4 μm (≈14000–2500 cm^{-1}). Figure 1(a) presents spectra obtained from silicon implanted at higher doses (1×10^{14} P^+/cm^2) and annealed at various temperatures. The low annealed sample (R300) already shows a certain trend of differentiation vis-a-vis the rest of the spectra. This trend is very obvious especially in the inset of Fig. 1(a). For the samples implanted at slightly higher dose: 5×10^{14} P^+/cm^2 [see Fig. 1(b)], unannealed and low annealed, one can see the increase of the fringe amplitude. The fringes of these samples and the ones presented in Figs. 1(b)–1(e) indicate that the materials implanted at high doses present, in optical terms—a bilayer form, while the implanted and high annealed materials seem more homogeneous.

For implantation doses equal to and over the critical dose Φ_c($\Phi_c=5\times10^{14}$ P^+/cm^2)[12] we note that in all the samples, except from those which have been annealed at very high temperatures (900 and 1100 °C), present interference fringe patterns form due to the amorphous/crystal layer [see Fig. 1(c)–1(e)]. It is also important to note that the fringe separation changes slightly with increasing implantation dose which is due to the fact that there is an increase in the difference between the reflective index of the two layers.

Beyond the fringe patterns which arise from interferences between light reflected by the front implanted surface and light reflected by the amorphized disorder-to-crystalline interface, Figs. 1(d) and 1(e) show some other very interesting features. In fact, for the highly annealed samples at longer wavelengths (between 3 and 4 μm) there appears to be a significant decrease in the reflection spectrum, and sometimes reflection minima. This phenomenon does not exist for the lower implanted samples. It is also important to note that in this infrared region, the variation of the reflectivity of the implanted and very highly annealed samples undergoes an anomalous dispersion. The same phenomenon has also been noted by Wang *et al.*[4] in implanted wafers. These authors have explained the phenomenon with the theory of plasma effect. In Figs. 1(d) and 1(e) we note that a characteristic minimum appears only for the samples annealed at 900 °C (R900). One would also expect to see such minimum on the highly annealed samples (1100 °C) as well, since it is well known that these possess more free carriers. Although this is true, Table I shows that these carriers are diffused in a very large thickness in the material and, thus, the number of free carriers per unit volume is lower than in the R900 sample. Finally, for those two samples annealed at 900 °C, one can note that the reflectivity minimum appears at lower wavelength, λ_p (≈3.1 μm), for the sample implanted at higher dose ($\Phi=1\times10^{16}$ P^+/cm^2) than for the sample implanted at lower dose ($\Phi=5\times10^{15}$ P^+/cm^2), $\lambda_p\approx3.5$ μm.

Note that in any case confusion should be avoided between reflectivity minima and interference fringes since for samples annealed at high temperatures (>600–700 °C) the interface amorphous-to-crystalline disappears. Therefore, there is no possibility of seeing any interference fringes from the samples annealed at 900 and 1100 °C from our samples in Fig. 1(e).

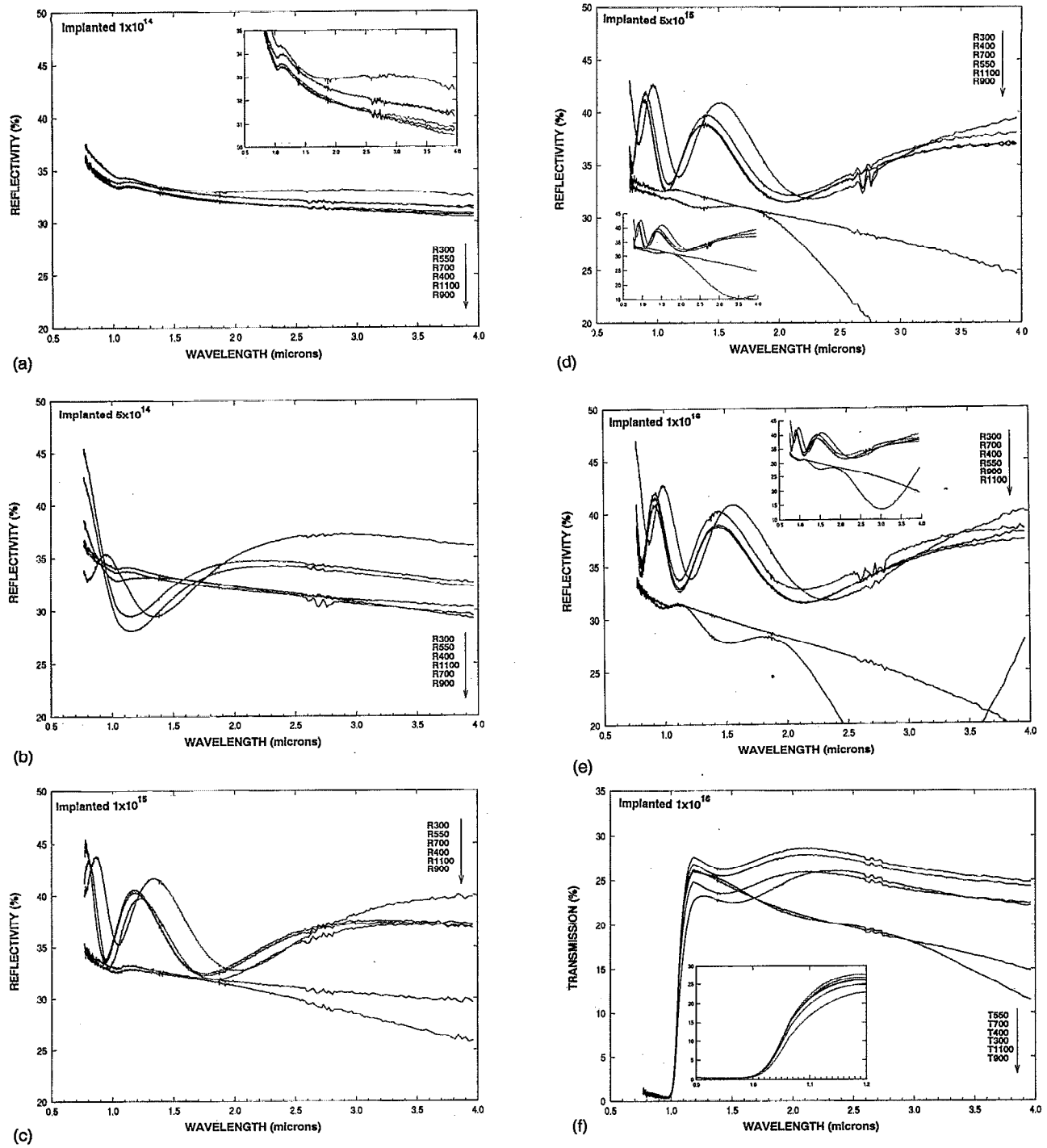

FIG. 1. FTIR reflection measurements of phosphorus implanted silicon wafers at various doses, $\Phi(P^+/cm^2)$: (a) 1×10^{14}, (b) 5×10^{14}, (c) 1×10^{15}, (d) 5×10^{15}, and (e) 1×10^{16} cm^{-2}. (f) FTIR transmission measurements of phosphorus implanted silicon wafers at doses $\Phi(P^+/cm^2)$: 1×10^{16}. Implantation energy: 150 keV. The samples were annealed isochronically (1 h) at various temperatures. Dashed line: nonimplanted sample.

Finally, Fig. 1(f) presents the transmission spectra of samples implanted at 1×10^{16} P^+/cm^2. We note that in the spectral range of 1–4 μm for samples annealed at 900 and 1100 °C both transmission [T, see Fig. 1(f)] and reflection [R: see Fig. 1(e)] decrease drastically. In fact as $T+R+A=1$ (where A is the optical absorptance) at 3.1 μm one can have: $A=1-T-R\approx0.69$, which is due to a very high absorption. This low absorptance can be explained only by the free carrier absorption phenomenon.

B. FTIR measurement between 3 and 25 μm

Figures 2(a)–2(f) present several FTIR transmission spectra obtained at room temperature in the range of 3.35–25 μm ($\approx$3000–400 cm^{-1}). For all the above figures the dip resulting from second-order absorption in pure c-Si bulk due to the silicon optic mode in the lattice is visible at around 15 μm. We note that first-order absorption is forbidden in silicon.[13]

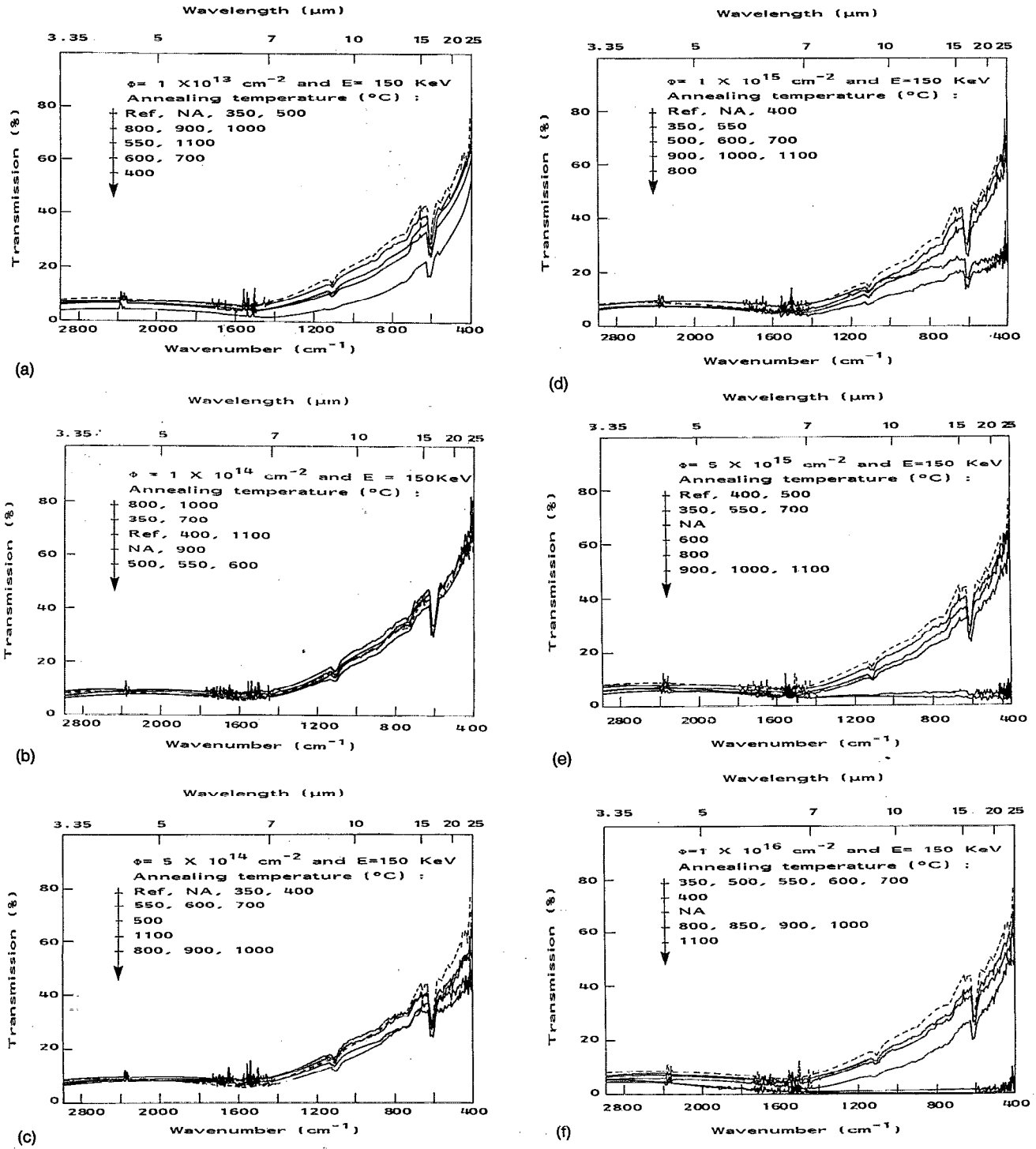

FIG. 2. FTIR transmission measurements of phosphorus implanted (E=150 keV) silicon wafers at various doses, $\Phi(P^+/cm^2)$: (a) 1×10^{13}, (b) 1×10^{14}, (c) 5×10^{14}, (d) 1×10^{15}, (e) 5×10^{15}, and (f) 1×10^{16}. The samples were annealed isochronically (1 h) at various temperatures. Dashed line: nonimplanted sample.

Figure 2(a) shows the behavior of a series of low implanted (1×10^{13} P^+/cm^2) and annealed samples. The dashed line refers to a nonimplanted sample. Note that the annealing temperatures, T_a, do not monotonically influence the variation of transmission versus λ. Nonmonotonic behavior is also observed for all samples implanted under the critical implantation dose, Φ_c. On the other hand, for the heavily implanted samples the transmission spectra change monotonically with annealing temperatures. For example, in Fig. 2(f) one can see that, with only exception of the unannealed sample, the transmission decreases with increasing T_a because of free carrier absorp-

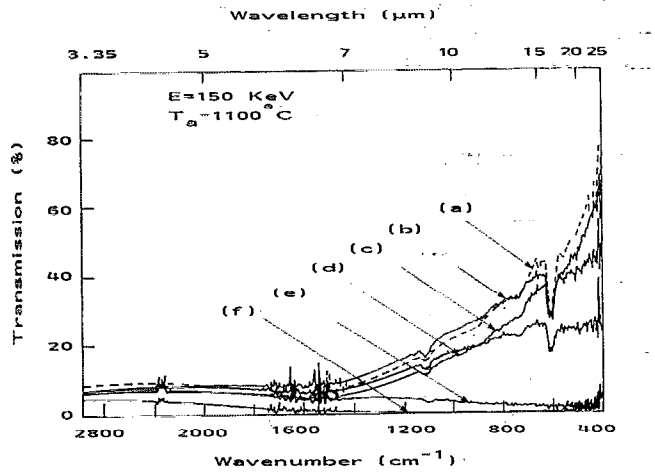

FIG. 3. FTIR transmission measurements of P^+ implanted silicon wafers (E=150 keV) at various doses, $\Phi(P^+/cm^2)$: (a) reference, (b) 1×10^{13} and 1×10^{14}, (c) 5×10^{14}, (d) 1×10^{15}, (e) 5×10^{15}, and (f) 1×10^{16}. The samples were annealed isochronically for 1 h at 1100 °C (data obtained from Fig. 2). Dashed line: nonimplanted sample.

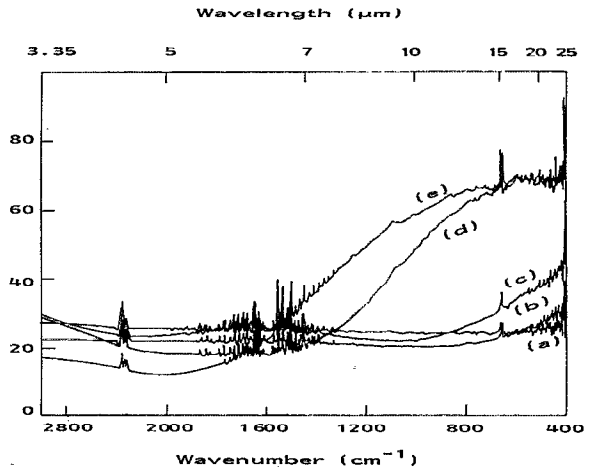

FIG. 4. FTIR reflection measurements of phosphorus implanted silicon wafers at various doses, $\Phi(P^+/cm^2)$: (a) 1×10^{13} and 1×10^{14}, (b) 5×10^{14}, (c) 1×10^{15}, (d) 5×10^{15}, and (e) 1×10^{16}. Implantation energy: 150 keV. The samples were annealed isochronically for 1 h at 1100 °C.

tion. For an annealing at 1100 °C the transmission spectrum is practically zero due to the high free carrier absorption.

From a critical comparison between Figs. 2(e) and 2(f) it is easy to note that for the heavily implanted samples (1×10^{16} P^+/cm^2) the transmission becomes almost zero only after annealing at 1100 °C, while the samples implanted with 5×10^{15} P^+/cm^2 show no transmission even after annealing at 900 °C. This confirms Gibbon's conclusion that the electrical activation of carriers decreases with increasing Φ.[14]

Figure 3 presents FTIR transmission measurements of phosphorus implanted silicon wafers at various implantation doses. The samples were annealed isochronically for 1 h at 1100 °C (data obtained from Fig. 2). One can see the strong dependence of optical transmission on the implanted phosphorus dose. In fact, we note that especially at long wavelengths (>7 μm) the transmission decreases as Φ increases.

The influence of implanted dose on FTIR reflection spectra for samples annealed isochronically for 1 h at 1100 °C is presented in Fig. 4. The low implanted samples do not present any minima, while for the rest of the spectra the wavelength position of the plasma edge, λ_p, shifts toward shorter wavelengths as the free carrier concentration increases. The same phenomenon has also been noted by Wagner and Schaefer for As^+ implanted silicon.[15]

Finally, Fig. 5 presents FTIR reflection measurements of heavily implanted (1×10^{16} P^+/cm^2) silicon wafers (unannealed and annealed) at various temperatures between 350 and 1100 °C. We note again a shift of the reflection minimum due to the variation of the free carriers as a function of the annealing temperature. For the unannealed and low annealed samples [Fig. 5, curves (a) and (b)] no minima are present.

IV. THEORETICAL BACKGROUND

The reflectivity minimum of FTIR spectra associated with plasma resonance has been an important tool for the determination of free carrier concentration in semiconductors for several years. A great deal of experimental and theoretical work has been carried out to improve and increase the accuracy of the calculation. One can cite, for example, the classical theoretical approach of Smith,[16] and the interesting development of this approach made by Schumann and Phillips.[12] The principal equations of Smith (in MKS) for the expression of the optical coefficients, n and k, were written as:

$$n^2-k^2=\frac{\epsilon_L}{\epsilon_0}-\frac{\sigma_0 e}{\mu_0\epsilon_0 m^*}\left\langle\frac{\tau^2}{1+\omega^2\tau^2}\right\rangle, \tag{1.1}$$

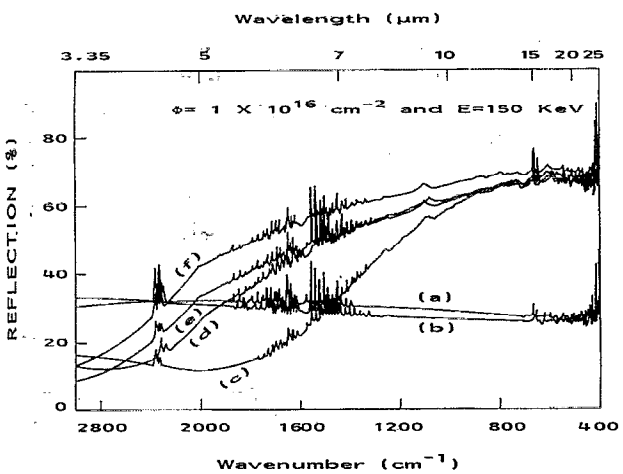

FIG. 5. FTIR reflection measurements of phosphorus implanted (1×10^{16} P^+/cm^2) silicon wafers at various temperatures, T_a(°C): (a) NA (nonannealed), 400, (b) 350, 500, 600, 700, (c) 1100, (d) 1000, (e) 800, (f) 900. Implantation energy: 150 keV.

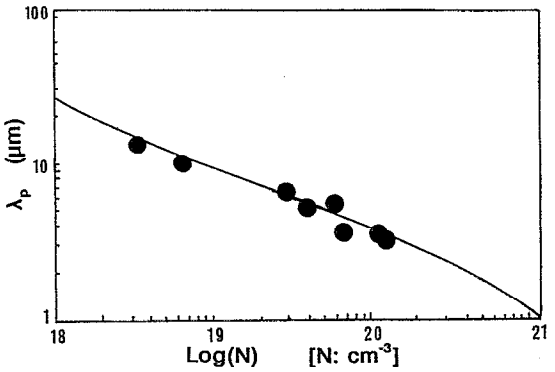

FIG. 6. The wavelength minimum reflectivity, λ_p vs the logarithm of carrier concentration, N. (Solid line): theoretical model of Schumann and Phillips (see Ref. 12), and experimental data taken from Figs. 1(d), 1(e), (4), and (5).

$$2nk=\frac{\sigma_0 e}{\omega\mu_0\epsilon_0 m^*}\left\langle\frac{\tau}{1+\omega^2\tau^2}\right\rangle, \tag{1.2}$$

where ϵ_L is the permittivity due to the lattice, σ_0 is the dc conductivity, μ_0 is the dc mobility, m^* is the conductivity of the effective mass, and τ is the relaxation time. Schumann and Phillips[12] have shown, under the assumption of nondegenerate statistics, that the above two equations can be written as:

$$n^2-k^2=\frac{\epsilon_L}{\epsilon_0}-\frac{\sigma_0\epsilon}{\mu_0\epsilon_0 m^*}\frac{\lambda^2}{4\pi^2c^2}J(D), \tag{2.1}$$

$$2nk=\frac{\sigma_0 e^4}{\mu_0\epsilon_0 m^{*2}}\frac{N\lambda^3\rho_0\Gamma(4)}{8\pi^3c^3[\Gamma(5/2)]^2}L(D), \tag{2.2}$$

where $J(D)$ and $L(D)$ are nondimensional and depend on the product $\omega^2\tau^2$. N is the carrier concentration, λ is the wavelength, ρ_0 the dc resistivity which is also a function of N (like μ_0), c the velocity of light in vacuum, and finally D is a function of N and λ.

According to Seeger, the approximation of small damping, where $\omega\tau\gg1$ is valid for most semiconductors even in the far-infrared spectrum.[17] As was pointed out by Schumann and Phillips[12] this is the approximation used most of the time and leads to $J(D)=L(D)=1$. Taking into account this approximation from the system of Eqs. (2.1) and (2.2) one can evaluate the index of refraction and the extinction coefficient k, both of them as a function of wavelength λ. The reflectivity was calculated from the well known expression:

$$R=\frac{(n-1)^2+k^2}{(n+1)^2+k^2}. \tag{3}$$

The minima in the reflectivity obtained from the derivative of the above equation are plotted in Fig. 6 (see solid line):

$$\frac{dR(\lambda)}{d\lambda}=0\rightarrow\lambda_p=\lambda_p(N,\mu_0,\rho_0,m^*). \tag{4}$$

For the numerical calculation, the effective mass was assumed to be 0.26. The value of resistivity as a function of carrier concentration has been obtained from various sources.[18,19] It is important to note that this model is valid for concentrations ranging between 1×10^{19} and 1×10^{21} cm^{-3}.

In the case of the application of this model to our implanted unannealed and annealed results the following points have to be taken into account: (a) The dc conductivity, σ_0 and mobility, μ_0 are dependent of the annealing temperatures;[20–22] (b) The conductivity of the effective mass, m^* depends on the degree of inhomogeneity of the material; and (c) ϵ is not constant for implanted silicon annealed at various temperatures.

V. DISCUSSION AND ANALYSIS

Figures 1(b)–1(e) clearly show that the increase of annealing temperature provokes a decrease of the fringe amplitude which indicates that the index of refraction was decreased during the isochronal annealing. In fact, the difference between the refractive index of implanted layers and substrate disappears as the annealing temperature increases. Samples implanted with 5×10^{14} P$^+$/cm^2 [see Fig. 1(b)] need only an annealing up to 550 °C for 1 h in order to make the fringes disappear, while annealing over 800 °C is necessary in the case of samples implanted at high doses. Using the data presented in Table I and the relation:

$$N(\text{cm}^{-3})=\frac{\phi(\text{cm}^{-2})}{d(\text{cm})} \tag{5}$$

the concentration of free carriers, N, is calculated. This concentration N assumes that all the implanted carriers are electrically active. d is the average value [$d\approx1/2(d_R+d_s)$ where d_R and d_s are the thicknesses of implanted layers obtained from spreading resistance and SUPREM III simulation, respectively] of the junction depth obtained by spreading resistance measurements and SUPREM III simulation.[23] In Table II one can find the concentration of free carriers for several implanted and highly annealed samples.

In Figs. 1(d) and 1(e) we note that a reflective minimum appears for samples annealed at 900 °C (R900). For these minima there is a corresponding plasma wavelength minimum which is proportional to[24]

$$\lambda_p\sim\sqrt{\frac{m^*}{16\pi^2e^2c^2N}}. \tag{6}$$

From Eq. (6) and Table I it is easy to understand why λ_p (of sample R900, 1×10^{16} P$^+$/cm^2) is smaller than λ_p (of sample R900, 5×10^{15} P$^+$/cm^2). The plasma wavelength λ_p of the samples annealed at 1100 °C are presented in longer wavelengths since their carriers per volume are smaller due to their high diffusion in the wafer.

Table II reports some experimental and theoretical data concerning 8 samples annealed at temperatures greater than 800 °C. In fact, in this table we also report the values of the junction depths (we report the average between the results obtained from SUPREM III simulation and spreading resistance measurements as well as each one separately), the free carrier impurities concentration N [ob-

TABLE II. Various values for 8 samples implanted and annealed at different conditions: (Φ) implantation dose, (T_a) annealing temperature, (N_R) "spreading" concentration of free carriers ($\approx\Phi/d_R$), (N_s) SUPREM concentration of free carriers ($\approx\Phi/d_s$), (N) average concentration of free carriers ($\approx\Phi/d$), and (λ_p) plasma wavelength taking into account the average free carriers concentration.

Φ (P^+/cm^2)	T_a (°C)	N_s (cm^{-3})	N_R (cm^{-3})	N (cm^{-3})	λ_p (μm)
5×10^{14}	1100	3.31×10^{18}	2.94×10^{18}	3.11×10^{18}	12.8
1×10^{15}	1100	6.58×10^{18}	5.74×10^{18}	6.13×10^{18}	10.5
5×10^{15}	1100	2.76×10^{19}	2.46×10^{19}	2.60×10^{19}	6.3
1×10^{16}	1100	4.16×10^{19}	3.86×10^{19}	4.00×10^{19}	5.0
1×10^{16}	1000	6.67×10^{19}	5.26×10^{19}	5.88×10^{19}	5.2
1×10^{16}	900	0.99×10^{20}	0.97×10^{20}	0.98×10^{20}	3.3
1×10^{16}	800	1.43×10^{20}	1.59×10^{18}	1.51×10^{20}	3.1
5×10^{15}	900	5.56×10^{18}	5.56×10^{18}	5.56×10^{19}	3.6

tained from Eq. (5)], the experimental plasma wavelength λ_p [data obtained from Figs. 1(d), 1(e), 4, and 5]. Figure 6 presents the plasma wavelength of the minimum reflectivity as a function of carrier concentration for n-type silicon. The solid line is obtained from the theoretical model presented in Sec. IV. In this figure one can see the good fitting of our experimental data taken from Figs. 1(d), 1(e), 4, and 5. Good agreement of the theory with the data, shows that $\omega^2\tau^2\gg1$ is a good approximation for implanted and highly annealed silicon wafers. On the other hand from these data one can conclude that only after annealing at 800 °C is there almost complete activation of implanted impurities. This is something which reconfirms the main results of the present authors obtained with Raman spectroscopy.[23]

It is also important to note that in Fig. 5 [curve (b)] even an annealing at 700 °C is not sufficient to activate the implanted impurities. In fact according to Eq. (5), where a complete activation is assumed, this sample possesses 1.88×10^{20} cm^{-3} carriers. In the case where 1% of these impurities were activated a reflectivity minimum would have appeared for $\lambda_p=20$ μm according to the Schumann and Phillips model.[12] This has not happened in our case. However, this conclusion is not completely realistic. As it is shown in Eq. (4), λ_p not only depends on the concentration N but also on the dc reflectivity and mobility, as well as the effective mass. In fact, according to the theoretical curve presented in Fig. 6, in the case where 1% of the carriers are activated (1.88×10^{18} cm^{-3}) a plasma wavelength of 20 μm corresponds to it. However, it should not be ignored that this theoretical curve corresponds to a completely crystalline silicon. Christofides *et al.*[20,21] and Othonos *et al.*[23] have shown, by performing electrical measurements, that dc conductivity and mobility vary even for annealing temperatures up to 700 °C. In our case annealing at 700 °C is probably not sufficient for a complete recrystallization. On the other hand the value of the effective mobility taken for this model (n-type crystalline silicon) may be different from that of an inhomogeneous material. Thus, the plasma wavelength in implanted and low annealed materials, which are not completely recrystallized, shifts to a longer wavelength. Electrical activation lower than 1% is no doubt an underestimation.

The last point which we believe is another important test of the theoretical model adopted in this study is to check whether the obtained carrier density corresponds to each experimental point λ_p of Fig. 6 by using the well known relation:

$$\mu_0=\frac{1}{e\rho_0 N}. \tag{7}$$

The dc mobility can be calculated by using the carrier density given in Table II and the spreading resistance data for the resistivity. Figure 7 shows the mobility as a function of the carrier density. The space included between the two solid lines corresponds to experimental data found by several researchers.[25] There is a close agreement between the experimental points obtained in this work and previously published data. A small disagreement with literature exists in experimental data obtained for samples annealed at temperatures lower than 1100 °C.

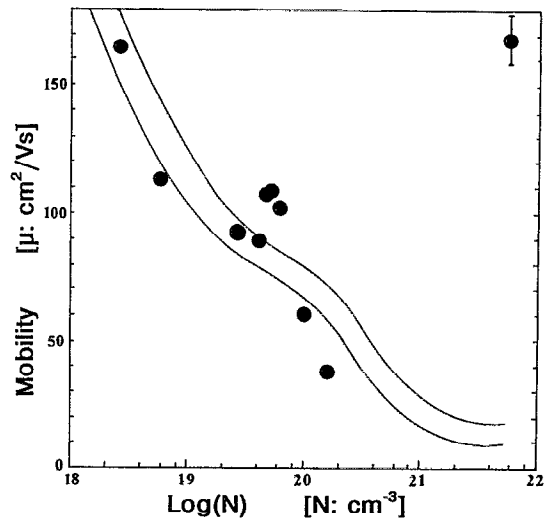

FIG. 7. Mobility as a function of the logarithm of carrier concentration.

VI. CONCLUSION

In conclusion, FTIR measurements at low wavelength can be used in order to obtain information concerning the influence of implantation dose and annealing temperature on the kinetics of reconstructions. From the interference fringes one can obtain information concerning the amorphous/crystal transition as a function of annealing temperature. From the presence of the absorption of free carriers in such samples one can obtain information concerning the electrical activation of these carriers. Finally, it has been shown that the classical model of Schumann and Phillips fits our experimental results very well. In fact, the fit of the plasma wavelength as a function of the free carriers shows that an annealing at 800 °C for 1 h is sufficient for a complete activation of carriers. On the other hand, it seems that the percentage of active carriers for highly implanted materials, even when annealed at 700 °C, is very low. This result shows that 550 °C is far from being the critical annealing temperature for a total recrystallization and complete electrical activation of carriers as was believed until today.[26]

[1] C. Christofides, Semicond. Sci. Technol. **7**, 1283 (1992).
[2] A. H. Kachare, W. G. Spitzer, J. E. Fredrickson, and F. K. Euler, J. Appl. Phys. **47**, 5374 (1976).
[3] A. H. Kachare, W. G. Spitzer, and J. E. Fredrickson, J. Appl. Phys. **47**, 4209 (1976).
[4] K-W. Wang, W. G. Spitzer, G. K. Hubler, and E. P. Donovan, J. Appl. Phys. **57**, 2739 (1985).
[5] G. K. Hubler, C N. Waddell, W. G. Spitzer, J. E. Fredrickson, S. Prussin, and R. G. Wilson, J. Appl. Phys. **50**, 3294 (1979).
[6] Sook-II Kwun, W. G. Spitzer, C. L. Anderson, H. L. Dunlap, and K. V. Vaidyanathan, J. Appl. Phys. **50**, 6873 (1979).
[7] G. K. Hubler, P. R. Malmberg, and T. P. Smith, J. Appl. Phys. **50**, 7147 (1979).
[8] J. E. Fredrickson, C. N. Waddell, W. G. Spitzer, and G. K. Hubler, Appl. Phys. Lett. **40**, 172 (1982).
[9] C. N. Waddell, W. G. Spitzer, G. K. Hubler, and J. E. Fredrickson, J. Appl. Phys. **53**, 5851 (1982).
[10] W. G. Spitzer, C. N. Waddell, G. H. Narayanan, J. E. Fredrickson, and S. Prussin, Appl. Phys. Lett. **30**, 623 (1977).
[11] J. Tatarkiewicz, Phys. Status Solidi B **153**, 11 (1989).
[12] P. A. Schumann, Jr. and R. P. Phillips, Solid State Electron. **10**, 943 (1967).
[13] H. Engstrom, J. Appl. Phys. **51**, 5245 (1980).
[14] J. F. Gibbons, Proc. IEEE **56**, 295 (1968).
[15] H. H. Wagner and R. R. Schaefer, J. Appl. Phys. **50**, 2697 (1979).
[16] R. A. Smith, *Semiconductors* (Cambridge University Press, Cambridge, 1959).
[17] K. Seeger, *Semiconductor Physics*, 4th ed., Springer Series in Solid State Sciences 40, edited by M. Cardona and H-J. Queisser (Springer, Berlin, 1988), Chap. 11.
[18] P. W. Chapman, O. N. Tufte, J. D. Zook, and D. Long, J. Appl. Phys. **34**, 3291 (1963).
[19] J. C. Irvin, Bell Syst. Tech. J. **41**, 387 (1962).
[20] C. Christofides, G. Guibaudo, and H. Jaouen, Revue Phys. Appl. **22**, 407 (1987).
[21] C. Christofides, G. Guibaudo, and H. Jaouen, J. Appl. Phys. **65**, 4840 (1989).
[22] C. Christofides, G. Guibaudo, and H. Jaouen, J. Appl. Phys. **65**, 4832 (1989).
[23] A. Othonos, C. Christofides, J. Boussey-Said, and M. Bisson (unpublished).
[24] P. Kireev, *The Physics of Semiconductors* (Mir, Moscow, 1975).
[25] G. Masetti, M. Severi, and S. Solmi, IEEE Trans. Electron Devices **ED-30**, 764 (1983).
[26] J. F. Gibbons, Proc. IEEE **60**, 1062 (1972).